GPS Solut (2010) 14:165–175
DOI 10.1007/s10291-009-0130-7

ORIGINAL ARTICLE

Low-degree earth deformation from reprocessed GPS observations

Mathias Fritsche · R. Dietrich · A. Rülke · M. Rothacher · P. Steigenberger

Received: 5 March 2009 / Accepted: 24 May 2009 / Published online: 12 June 2009

Abstract Surface mass variations of low spherical harmonic degree are derived from residual displacements of continuously tracking global positioning system (GPS) sites. Reprocessed GPS observations of 14 years are adjusted to obtain surface load coefficients up to degree $n_{\max} = 6$ together with station positions and velocities from a rigorous parameter combination. Amplitude and phase estimates of the degree-1 annual variations are partly in good agreement with previously published results, but also show interannual differences of up to 2 mm and about 30 days, respectively. The results of this paper reveal significant impacts from different GPS observation modeling approaches on estimated degree-1 coefficients. We obtain displacements of the center of figure (CF) relative to the center of mass (CM), $\Delta\mathbf{r}_{\mathrm{CF-CM}}$, that differ by about 10 mm in maximum when compared to those of the commonly used coordinate residual approach. Neglected higher-order ionospheric terms are found to induce artificial seasonal and long-term variations especially for the z-component of $\Delta\mathbf{r}_{\mathrm{CF-CM}}$. Daily degree-1 estimates are examined in the frequency domain to assess alias contributions from model deficiencies with regard to satellite orbits. Finally, we directly compare our estimated low-degree surface load coefficients with recent results that involve data from the Gravity Recovery and Climate Experiment (GRACE) satellite mission.

Keywords GPS · Surface mass redistribution · Terrestrial reference frame

M. Fritsche (✉) · R. Dietrich · A. Rülke
Institut für Planetare Geodäsie, Technische Universität Dresden, 01062 Dresden, Germany
e-mail: fritsche@ipg.geo.tu-dresden.de

M. Rothacher
Institut für Geodäsie und Photogrammetrie, Eidgenössische Technische Hochschule Zürich, 8093 Zurich, Switzerland

P. Steigenberger
Institut für Astronomische und Physikalische Geodäsie, Technische Universität München, 80290 Munich, Germany

Introduction

The definition and realization of a terrestrial reference system (TRS) is a basic prerequisite for global geodetic and geodynamic applications. It plays a fundamental role in the study of global deformation and mass exchange processes in the earth system which are the main focus of the global geodetic observing system (GGOS) (Drewes 2007). Space geodetic observations are of special interest in order to derive the associated terrestrial reference frame (TRF). The origin of the International Terrestrial Reference System (ITRS) is defined to be the center of mass of the earth system (CM), including oceans, atmosphere and continental water (McCarthy and Petit 2004). Since this center is directly related to satellite orbital motion, it is the most appropriate choice to model satellite geodetic measurements. Crustal deformations caused by mass redistribution within the earth's system displace the solid earth crust with respect to the CM. Taking these load-induced variations of site positions into consideration, there is the important requirement that any realization of a TRS must ensure a self-consistent description of surface load deformation and the chosen reference frame origin (Blewitt 2003).

The International Terrestrial Reference Frame (ITRF) is a realization of the ITRS (Altamimi et al. 2007). In this realization, the effects of several mass load changes have not yet been taken into account, such as changes

originating from atmosphere or continental water. Viewed in the long term, the site coordinates relate to the CM because crustal deformations of seasonal origin are expected to cancel. However, load-induced deformations displace the solid earth crust relative to the CM. Since site coordinates are used to approximate the earth's surface, it follows that the associated center of figure (CF) deviates from the CM on shorter time scales. Thus, a conflict remains between desirable and the realizable properties of the ITRF (Dong et al. 2003). However, in the absence of high-accurate reduction models, the treatment of residual load-induced deformation signals as estimable quantities in the adjustment procedure ensures a self-consistent description between the origin of the frame and loading dynamics (Dong et al. 2003).

Based on least-squares inversion of weekly global positioning system (GPS) solutions published by the International GNSS Service (IGS) (Dow et al. 2005), several authors proposed and applied different approaches in order to solve for the degree-1 spherical harmonics of the redistributed surface load (Heflin and Watkins 1999; Blewitt et al. 2001; Dong et al. 2003). The unified modeling of site displacements in a CM frame is shown to be the most consistent way for describing space geodetic observations (Lavallée et al. 2006). In order to circumvent the drawbacks resulting from sparse number of network sites in ocean areas and from heterogeneous distribution of continental sites, constrained inversion methods are applied to GPS observations, e.g., by Kusche and Schrama (2005) and Wu et al. (2006). Their inversion schemes incorporate a priori information from model data or satellite data from the gravity recovery and climate experiment (GRACE). In contrast, Clarke et al. (2007) estimate the surface load over land using a regional base function approach. Their modified base functions provide a self-consistent description of the variable load over land, global mass conservation and equilibrium tidal behavior of the oceans. This representation is found to achieve a better fit to realistic synthetic data than estimates of standard spherical harmonics with the same degree of expansion. However, reasonable good a priori information on the real load distribution is essential for the formulation of the modified set of base functions.

Estimates of the surface mass variability inferred from geodetic measurements of load-induced crustal deformation are essential for complementing satellite gravimetry data (e.g., Davis et al. 2004; van Dam et al. 2007). In case a combination of parameters from different techniques is preferred, deficiencies in systematic observation modeling will bias the combined product. Shortcomings arising from incomplete coverage of the earth's surface by the GPS network are already successfully accounted for, as stated above. Other known systematic deficiencies have not been discussed yet in detail. In particular, none of the approaches applied so far have been investigated in terms of realizing the TRS, although surface load related degree-1 coefficients are crucial in this context. Rülke et al. (2008) applied for the first time a rigorous parameter combination approach in order to determine a TRF using the reprocessed GPS observations from a global network discussed in Steigenberger et al. (2006). In continuation of that work, this paper focuses on the investigation of spherical harmonic degree-1 earth deformation. In particular, we will evaluate potential biases originating from technique-specific modeling aspects such as the higher-order ionospheric terms and the solar radiation pressure that is acting on the GPS satellites. Finally, we compare the resulting low-degree load coefficients with corresponding products from GRACE.

Surface load estimation

The interaction between the TRF and loading dynamics is described following the formalism of Blewitt (2003), where the load-induced topocentric displacement vector **s** (local directions north, east, up) of a point with latitude φ and longitude λ is:

$$
\begin{aligned}
s_n(\varphi,\lambda) &= \frac{4\lambda R_E^3}{M_E}\sum_{n=1}^{\infty}\sum_{m=0}^{n}\sum_{\Phi}^{\{C,S\}}\frac{l'_n\,\sigma_{nm}^{\Phi}}{2n+1}\partial_{\varphi}\,\mathrm{Y}_{nm}^{\Phi}(\varphi,\lambda)\\
s_e(\varphi,\lambda) &= \frac{4\lambda R_E^3}{M_E}\sum_{n=1}^{\infty}\sum_{m=0}^{n}\sum_{\Phi}^{\{C,S\}}\frac{l'_n\,\sigma_{nm}^{\Phi}}{2n+1}\frac{\partial_{\lambda}\,\mathrm{Y}_{nm}^{\Phi}(\varphi,\lambda)}{\cos\varphi}\\
s_u(\varphi,\lambda) &= \frac{4\lambda R_E^3}{M_E}\sum_{n=1}^{\infty}\sum_{m=0}^{n}\sum_{\Phi}^{\{C,S\}}\frac{h'_n\,\sigma_{nm}^{\Phi}}{2n+1}\mathrm{Y}_{nm}^{\Phi}(\varphi,\lambda)
\end{aligned}
\qquad (1)
$$

In Eq. 1 the symbol σ_{nm}^{Φ} denotes the spherical harmonic coefficients of the surface load density, $\Phi \in \{C, S\}$ where C and S identify the cosine and sine expansion components, Y_{nm}^{Φ} are the spherical harmonic base functions of degree n and order m, and l'_n and h'_n denote the degree-dependent load Love numbers. The mass and mean radius of the earth is denoted by M_E and R_E.

Normal equation system expansion

Usually, a model of station positions changing linear with time is adopted for the realization of the TRS. In order to account for the load-induced deformation as a time- and frame-dependent correction, the linear least-squares solution is expanded. Accordingly, the parameter vector **u** applied for the TRS realization is composed as follows:

$$
\mathbf{u} = [\,\mathbf{x} \quad \mathbf{p} \quad \boldsymbol{\sigma}\,]^T \qquad (2)
$$

With station coordinates and station velocities **x**, common geophysical (earth rotation) and technique-specific

(satellite orbit) parameters $\mathbf{p}$, and surface load coefficients $\boldsymbol{\sigma}$, the least-squares design matrix reads

$$\mathbf{A} = \begin{bmatrix} \frac{\partial \mathbf{l}}{\partial \mathbf{x}} & \frac{\partial \mathbf{l}}{\partial \mathbf{p}} & \frac{\partial \mathbf{l}}{\partial \boldsymbol{\sigma}} \end{bmatrix} \tag{3}$$

Denoting the inverse of the covariance of the observations $\mathbf{l}$ by $\mathbf{P}$, the matrix $\mathbf{N}$ and vector $\mathbf{b}$ of the normal equation system become

$$\begin{aligned} \mathbf{N} = \mathbf{A}^T\mathbf{P}\mathbf{A} &= \begin{bmatrix} \mathbf{N}_{\mathbf{xx}} & \mathbf{N}_{\mathbf{xp}} & \mathbf{N}_{\mathbf{x}\sigma} \\ \cdots & \mathbf{N}_{\mathbf{pp}} & \mathbf{N}_{\mathbf{p}\sigma} \\ \cdots & \cdots & \mathbf{N}_{\sigma\sigma} \end{bmatrix} \\ &= \begin{bmatrix} \frac{\partial \mathbf{l}}{\partial \mathbf{x}}^T\mathbf{P}\frac{\partial \mathbf{l}}{\partial \mathbf{x}} & \frac{\partial \mathbf{l}}{\partial \mathbf{x}}^T\mathbf{P}\frac{\partial \mathbf{l}}{\partial \mathbf{p}} & \frac{\partial \mathbf{l}}{\partial \mathbf{x}}^T\mathbf{P}\frac{\partial \mathbf{l}}{\partial \boldsymbol{\sigma}} \\ \cdots & \frac{\partial \mathbf{l}}{\partial \mathbf{p}}^T\mathbf{P}\frac{\partial \mathbf{l}}{\partial \mathbf{p}} & \frac{\partial \mathbf{l}}{\partial \mathbf{p}}^T\mathbf{P}\frac{\partial \mathbf{l}}{\partial \boldsymbol{\sigma}} \\ \cdots & \cdots & \frac{\partial \mathbf{l}}{\partial \boldsymbol{\sigma}}^T\mathbf{P}\frac{\partial \mathbf{l}}{\partial \boldsymbol{\sigma}} \end{bmatrix} \\ \mathbf{b} = \mathbf{A}^T\mathbf{P}\mathbf{l} &= [\mathbf{b}_{\mathbf{x}} \quad \mathbf{b}_{\mathbf{p}} \quad \mathbf{b}_{\boldsymbol{\sigma}}]^T = \begin{bmatrix} \frac{\partial \mathbf{l}}{\partial \mathbf{x}}^T\mathbf{P}\mathbf{l} & \frac{\partial \mathbf{l}}{\partial \mathbf{p}}^T\mathbf{P}\mathbf{l} & \frac{\partial \mathbf{l}}{\partial \boldsymbol{\sigma}}^T\mathbf{P}\mathbf{l} \end{bmatrix} \end{aligned} \tag{4}$$

The partial derivatives $\partial\mathbf{l}/\partial\boldsymbol{\sigma}$ refer to a geocentric cartesian coordinate system and can be reformulated as following:

$$\frac{\partial \mathbf{l}}{\partial \boldsymbol{\sigma}} = \frac{\partial \mathbf{l}}{\partial \mathbf{x}}\frac{\partial \mathbf{x}}{\partial \boldsymbol{\sigma}} = \frac{\partial \mathbf{l}}{\partial \mathbf{x}} diag[\mathbf{R}_1 \quad \ldots \quad \mathbf{R}_k]\frac{\partial \mathbf{s}}{\partial \boldsymbol{\sigma}} \tag{5}$$

where $\partial\mathbf{x}/\partial\boldsymbol{\sigma}$ denotes the derivative of the coordinate derivatives with respect to the surface load coefficients. The derivatives of load-induced displacements with respect to the surface load coefficients $\partial\mathbf{s}/\partial\boldsymbol{\sigma}$ can easily be derived from Eq. 1 and then transformed by the 3×3 rotation matrices

$$\mathbf{R}_i = \begin{bmatrix} -\sin\varphi_i\cos\lambda_i & -\sin\lambda_i & \cos\varphi_i\cos\lambda_i \\ -\sin\varphi_i\sin\lambda_i & \cos\lambda_i & \cos\varphi_i\sin\lambda_i \\ \cos\varphi_i & 0 & \sin\varphi_i \end{bmatrix} \tag{6}$$

into the geocentric system for each site ($i = 1 \ldots k$). Using Eq. 5 to express all relevant elements of the normal equations in Eq. 4 in terms of $\partial\mathbf{x}/\partial\boldsymbol{\sigma}$ leads to

$$\begin{aligned} \mathbf{N}_{\mathbf{x}\sigma} &= \frac{\partial \mathbf{l}}{\partial \mathbf{x}}^T\mathbf{P}\frac{\partial \mathbf{l}}{\partial \mathbf{x}}\frac{\partial \mathbf{x}}{\partial \boldsymbol{\sigma}} = \mathbf{N}_{\mathbf{xx}}\frac{\partial \mathbf{x}}{\partial \boldsymbol{\sigma}} \\ \mathbf{N}_{\mathbf{p}\sigma} &= \frac{\partial \mathbf{l}}{\partial \mathbf{p}}^T\mathbf{P}\frac{\partial \mathbf{l}}{\partial \mathbf{x}}\frac{\partial \mathbf{x}}{\partial \boldsymbol{\sigma}} = \mathbf{N}_{\mathbf{xp}}^T\frac{\partial \mathbf{x}}{\partial \boldsymbol{\sigma}} \\ \mathbf{N}_{\sigma\sigma} &= \frac{\partial \mathbf{x}}{\partial \boldsymbol{\sigma}}^T\frac{\partial \mathbf{l}}{\partial \mathbf{x}}^T\mathbf{P}\frac{\partial \mathbf{l}}{\partial \mathbf{x}}\frac{\partial \mathbf{x}}{\partial \boldsymbol{\sigma}} = \frac{\partial \mathbf{x}}{\partial \boldsymbol{\sigma}}^T\mathbf{N}_{\mathbf{xx}}\frac{\partial \mathbf{x}}{\partial \boldsymbol{\sigma}} \\ \mathbf{b}_{\boldsymbol{\sigma}} &= \frac{\partial \mathbf{x}}{\partial \boldsymbol{\sigma}}^T\frac{\partial \mathbf{l}}{\partial \mathbf{x}}^T\mathbf{P}\mathbf{l} = \frac{\partial \mathbf{x}}{\partial \boldsymbol{\sigma}}^T\mathbf{b}_{\mathbf{x}} \end{aligned} \tag{7}$$

These relations reveal two important properties. First, all parts of the normal equations that contain the new parameters $\boldsymbol{\sigma}$ are decomposable based on existing normal equation elements as long as all the coordinate-related parameters $\mathbf{x}$ are explicitly given. Second, taking into account a mean position for each site, the individual site-specific partial derivates $\partial\mathbf{x}/\partial\boldsymbol{\sigma}$ are constant. This allows the setting up of these additional coefficients at the normal equation level, assuming that the observation time interval, represented by $\mathbf{b}_x$, coincides with the validity interval of the parameters $\boldsymbol{\sigma}$ (i.e., it is sufficient to expand and combine daily normal equations if weekly load coefficients are of interest).

Reference system realization

A basic precondition of the investigations presented in this paper is the determination of a GPS-only realization of the ITRS following the approach described by Rülke et al. (2008). Consequently, site-specific surface displacements are modeled based on Eq. 1 with degree-1 load Love numbers in the CM frame. We modified the Bernese GPS Software version 5.0 (Dach et al. 2007) to set up surface load coefficients as continuous piecewise-linear functions according to Eq. 7, producing daily normal equation systems. These are then combined to simultaneously solve for station coordinates $\mathbf{x}$ and velocities $\dot{\mathbf{x}}$ together with pole coordinates x_p and y_p, and surface load coefficients $\boldsymbol{\sigma}$. In order to avoid aliasing errors that originate from unmodeled higher-degree loading (Wu et al. 2002), the spherical harmonic degree $n_{\max}$ is set to 6 maximum. Figure 1 (top) gives an overview of the evolution of the number of network sites and the percentage of sites on the positive part of the x-, y- and z-axis. Although the total number of sites increases with time, an uneven distribution between the northern and southern hemisphere remains. To account for the effective number of contributing sites, the maximum degree in Eq. 1 is incremented from $n_{\max} = 2$ in 1994.0 to $n_{\max} = 6$ in 1998.0 as shown in Fig. 1 (bottom).

To invert the rank-deficient accumulated normal equation matrix of the final solution, additional no-net-rotation conditions are applied with respect to the station network orientation and the respective orientation rate. In the presence of site coordinates, additional rank-deficits are caused by the simultaneous estimation of surface load coefficients. These are caused by the fact that the mean of each type of coefficient σ_{nm}^{Φ} corresponds to a constant coordinate displacement field. The same principle is true for the respective linear changes. Thus, additional minimum constraint conditions are imposed on each series of σ_{nm}^{Φ} coefficients such that the related mean and linear change have zero mean with respect to the whole combination period of 14 years (cf. Rülke et al. 2008).

Results

The global GPS solutions are the outcome of a reprocessing effort of Technische Universität Dresden, Technische Universität München and GeoForschungsZentrum

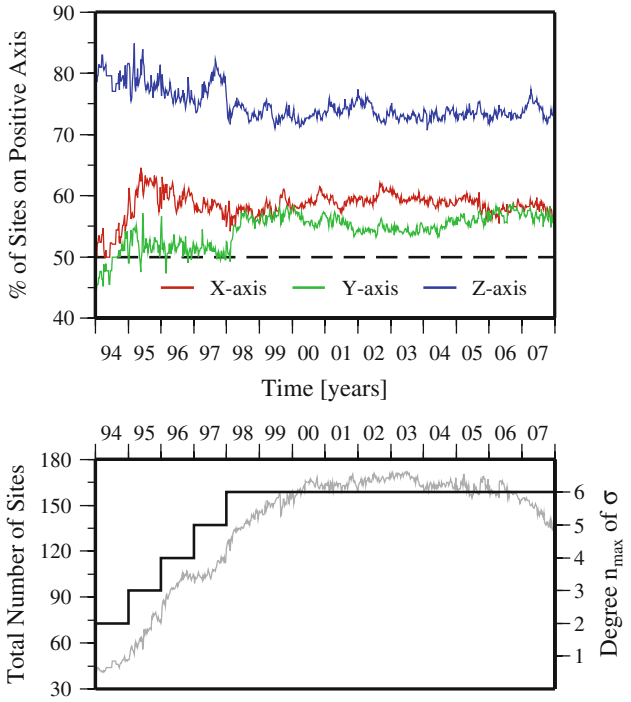

Fig. 1 Number of sites versus maximum spherical harmonic degree. The *top panel* shows weekly number of sites used in the reprocessing and associated percentage of sites in the hemisphere centered on positive *x*-, *y*- and *z*-axis. The *bottom panel* shows the total number of sites and the maximum spherical harmonic degree $n_{\max}$ (*solid line*) used for the surface load density estimation

Potsdam. In this paper, we make use of solutions based on the latest computation. In comparison to Steigenberger et al. (2006) the observations are analyzed with an updated processing scheme. For some of the results discussed in this section operations on the normal equation level are performed, e.g., parameter stacking regarding any interval length. Furthermore, we will discuss the impact of different observation modeling approaches. In these cases, the results refer to separate observation adjustments where all options were left unchanged except the model component of interest.

Rigorous combination approach

The results of a rigorous combination approach include data over the period from 26 December 1993 to 5 January 2008. We apply the procedure as described above, where the surface load coefficients are finally transformed to equidistant epochs at 28-day interval boundaries. For reasons of comparison, continuous piecewise-linear parameter estimates are used to derive interpolated values that refer to the center of the interval of subsequent parameter epochs. This is equivalent to an approach that considers offset estimates of an offset/drift parameterization with an enforced continuity between subsequent parameter intervals. Corresponding degree-1 values from 14 years of data are shown in Fig. 2 (black line). These are the basis for further investigations. The degree-1 coefficients are converted to the vector difference $\Delta\mathbf{r}_{\mathrm{CF-CM}}$ according to Blewitt (2003). This conversion represents the translation of the CF frame with respect to the CM frame. The displacement between both origins amounts to about 1 cm maximum. An empirical model including an annual and a semiannual part is then determined for each component. Related amplitude and phase estimates are summarized in Table 1. We find that an annual variation is dominant in the *z*- and in *y*-translation. Subtracting the empirical annual part from the obtained time series reduces the variance by 52 and 34%, respectively. A strong annual signal for the *x*-translation is not evident, which is confirmed by the fact that the signal variance is only slightly reduced. The semiannual fraction, in contrast, accounts for not more than 2% of the signal variance for all components. Compared to other studies compiled in Table 1, our amplitudes in *x* and *y* are the smallest, whereas related phase estimates agree well within the range of other solutions. With regard to the *z*-component, our estimate for the amplitude is on the lower bound, whereas again the phase shows a good agreement with previously published results.

Coordinate residual approach

In contrast to the rigorous adjustment for surface load coefficients, the coordinate residual approach is a two-step strategy. A reference solution composed of mean station coordinates and velocities is derived first using all observations. In the second step, the coordinate estimates based on subsets of observations (e.g., weekly solutions) are compared with the reference solution. The coordinate residuals obtained are then propagated to surface load coefficients (Blewitt et al. 2001; Wu et al. 2003; Kusche and Schrama 2005; Lavallée et al. 2006). In this case, the correlations between surface load coefficients from neighboring intervals and the correlations with other parameter types that are taken into account by the rigorous formulation (Eq. 7) are neglected. Moreover, the coefficients obtained represent average values valid over the time interval of the individual solution. In the second step, we do not adjust for additional network translation parameters. Therefore, the solutions for both the reference frame and the subset frames use the direct satellite orbit information on the CM.

For comparison purposes, we also applied the coordinate residual approach to reprocessed observations. The resulting coefficients are valid for an interval length of 28 days and are shown in Fig. 2 (gray line). The largest differences compared to the rigorous solution are obtained for the σ_{10}^{C}-component, mainly resulting in larger amplitude during

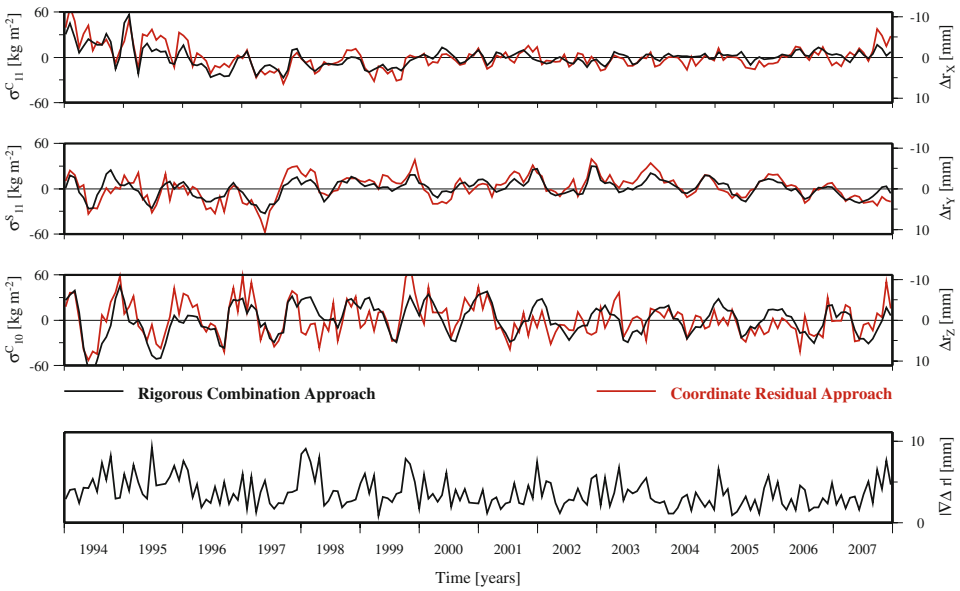

Fig. 2 Degree-1 surface load estimates. The *top three panels* show degree-1 surface load estimates from 14 years of GPS data from a rigorous parameter combination approach (*black*) and a coordinate residual approach (*red*). The estimates refer to 28-day intervals. *Right hand scale* gives the displacement of the CF relative to the CM. The *bottom panel* shows the magnitude of difference between both estimation approaches

Table 1 Amplitude and phase estimates for annual and semiannual variations of CF displacement relative to the CM

	Approach[c]	n_{max}^{d}	Time span	Amplitude[a] (A, mm) and phase (Φ, days) of $\Delta\mathbf{r}_{CF-CM}^{b}$					
				x		y		z	
				A	Φ	A	Φ	A	Φ
Annual									
Blewitt et al. (2001)[e]	D1A	1	1996.00–2001.00	3.4 ± 0.3	270 ± 3	5.0 ± 0.3	167 ± 3	11.3 ± 0.2	239 ± 1
Dong et al. (2003)[e]	D1A	1	1993.00–2002.87	2.1 ± 0.3	229 ± 7	3.3 ± 0.3	155 ± 6	7.1 ± 0.3	221 ± 3
Wu et al. (2003)[e]	D1A	6	1997.00–2002.00	0.7 ± 1.5	302 ± 131	3.8 ± 1.2	199 ± 20	4.5 ± 1.0	210 ± 13
Lavallée et al. (2006)[e]	CM	2	1997.25–2004.25	2.1 ± 0.6	222 ± 21	3.2 ± 0.5	163 ± 22	3.9 ± 0.8	257 ± 22
Kusche et al. (2005)	CIM	7	1999.48–2004.48	3.9	205	2.7	208	7.6	240
Wu et al. (2006)[e]	CIM	50	1999.00–2004.25	1.7 ± 0.3	173 ± 11	3.8 ± 0.3	162 ± 4	4.5 ± 0.3	204 ± 4
This study	CM	6	1994.00–2008.00	0.1 ± 0.2	222 ± 93	1.8 ± 0.2	159 ± 11	4.0 ± 0.2	205 ± 6
Semiannual									
Blewitt et al. (2001)[e]	D1A	1	1996.00–2001.00	1.2 ± 0.3	126 ± 13	1.0 ± 0.3	61 ± 13	2.6 ± 0.2	14 ± 5
Wu et al. (2003)[e]	D1A	6	1997.00–2002.00	1.2 ± 1.5	138 ± 37	1.9 ± 1.2	69 ± 20	1.6 ± 1.0	156 ± 18
Wu et al. (2006)[e]	CIM	50	1999.00–2004.25	1.0 ± 0.3	27 ± 9	0.9 ± 0.3	52 ± 10	0.6 ± 0.3	22 ± 15
This study	CM	6	1994.00–2008.00	0.5 ± 0.2	60 ± 9	0.2 ± 0.2	40 ± 24	0.5 ± 0.2	24 ± 10

[a] Amplitude and phase are defined by $A\cos[\omega(t - t_0 - \Phi)]$ where t_0 is first January and Φ the phase

[b] CF is center of figure; CM is center of mass

[c] D1A: degree-1 approach, CM: center of mass approach, CIM: constrained inversion method

[d] Maximum degree of spherical harmonic expansion

[e] Amplitude and/or phase results are converted to conform to the required conventions

the first years of the time series and with a generally increased variability. The absolute differences for $\Delta\mathbf{r}_{CF-CM}$ are 3.7 mm on average and amount to 10 mm maximum.

Degree-1 annual variation

When comparing amplitudes and phases from Table 1, all studies are limited to the range of $1 \leq n_{max} \leq 6$ except for those including additional a priori information from GRACE satellite data and ocean bottom pressure obtained from an oceanic circulation model (Kusche and Schrama 2005; Wu et al. 2006). Figure 3 shows the annual amplitude and phase estimates, each set based on degree-1 results derived from individual TRS realizations, where all options but the degree of truncation n_{max} were left unchanged. The largest differences in amplitude are about 1.0 mm in x and y and 1.5 mm in z. Phase estimates differ by about 30 days in x as well as 10 days in y and z.

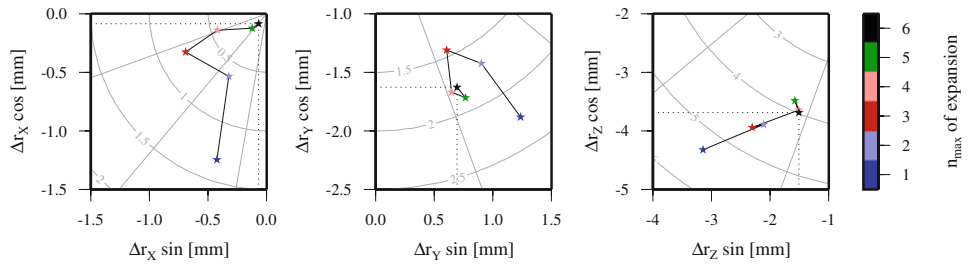

Fig. 3 Cosine and sine amplitudes for an annual variation of degree-1 surface load components converted to $\Delta\mathbf{r}_{\mathrm{CF-CM}}$ based on 14 years of data. The *color* indicates the maximum spherical harmonic degree $n_{\max}$ to which the separate realizations of the terrestrial reference system refer. *Isolines* indicate amplitudes and equidistant phase steps of 30° (≈30.4 days)

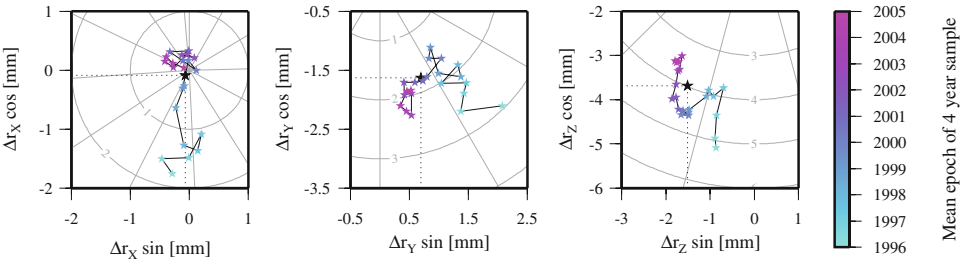

Fig. 4 Cosine and sine amplitudes for an annual variation of degree-1 surface load components converted to $\Delta\mathbf{r}_{\mathrm{CF-CM}}$ based on time series samples with a 4-year interval length successively shifted by half a year. The *color* indicates the mean epoch of each sample. *Isolines* indicate amplitudes and equidistant phase steps of 30° (≈30.4 days). Estimates with respect to the reference solutions spanning 14 years of data are represented by *black stars*

Applying $4 \leq n_{\max} \leq 6$ gives similar results. This effect is known to be caused by the aliasing effect from higher-degree loading (Wu et al. 2002) and complicates a simple comparison of results stemming from studies with different degrees of truncation.

Various time spans of input data have been considered for the investigations listed in Table 1. Accordingly, we generated samples of degree-1 time series with an interval length of 4 years, each successively shifted by half a year. A comparison of associated amplitudes and phases in Fig. 4 reveals that an interannual variability is evident for both. The differences are in the order of 1−2 mm for the amplitudes. The phases differ by about 30 days for the *y*- and *z*-component. The phase in *x* reveals the largest uncertainty with respect to the selected input time span. However, larger discrepancies for sample intervals of earlier years are probably due to the sparser network.

Higher-order ionospheric effects

Dual-frequency GPS observables which are used to formulate the quasi ionosphere-free linear combination allow the elimination of the first-order ionospheric effect. Neglecting second and third-order ionospheric correction terms induce artificial deviations for a number of GPS derived estimates (Fritsche et al. 2005). In Table 1 only the results of our study include these higher-order observation corrections. A separate analysis is performed in order to assess the impact of this modeling difference on the derived degree-1 estimates. We compute the differences between weekly standard solutions, where the second and third-order ionospheric corrections are applied, and modified weekly solutions that account for the first-order term only. Since a more detailed coordinate residual pattern can be represented as the degree of truncation of the spherical harmonic expansion increases, the degree-1 differences are evaluated depending on $n_{\max}$. Due to the increased number of unknown parameters (weekly vs. 28 days), the standard and modified solutions were derived according to the coordinate residual approach (see "Coordinate residual approach").

Figure 5a illustrates the total electron content (TEC) of the ionosphere exhibiting the characteristic solar cycle of about 11 years and semiannual variations. As a first approximation, the magnetic field of the earth can be described by a dipole model which causes the largest corrections in magnitude for observations that coincide with the dipole's meridian plane. Consequently, predominant station coordinate residuals would be obtained for the north and up component as shown in Fig. 5b. These artificial coordinate residuals are partly mapped into the coefficients of the spherical harmonic expansion of Eq. 1. The differences obtained for weekly degree-1 coefficients are shown in Fig. 5c–e. The zero line represents results obtained when accounting for the higher-order ionospheric

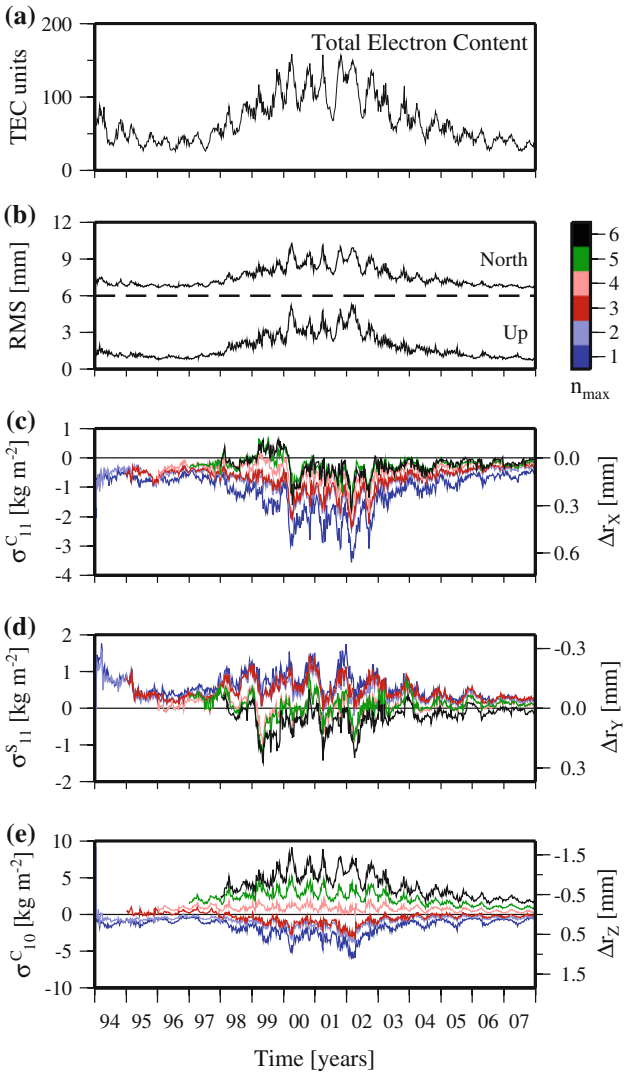

Fig. 5 Comparison of modified and standard solutions. Panel **a** shows the TEC of the ionosphere represented by weekly averages of the mean electron density. Panel **b** shows the RMS of artificial site displacements induced by second- and third-order ionospheric terms for up and north (shifted by 6 mm). Panels **c–e** show the differences of weekly degree-1 estimates between modified solutions (first-order ionospheric term only) and standard solutions (second- and third-order ionospheric terms in addition). The *color* indicates the maximum spherical harmonic degree $n_{\max}$ used for the surface load density estimation

terms. Positive values refer to larger estimates obtained for the modified solutions which include the first-order ionospheric term only. Figure 5c shows that σ_{11}^{C}-estimates are less biased for $n_{\max} = 6$ than for $n_{\max} = 2$. No such clear distinction can be made for the σ_{11}^{S}-estimates though the absolute values are small. The largest differences in magnitude are obtained for the σ_{10}^{C}-coefficient corresponding to an artificial z-translation in $\Delta\mathbf{r}_{\mathrm{CF-CM}}$ of about 1.5 mm in maximum (see Fig. 5e). It is interesting to note that an identical approach, limited to $n_{\max} = 1$, results in values of almost the same magnitude but opposite in sign. Thus, the systematic difference can reach the amount of 2.5 mm during periods of a solar maximum. Since the other studies neglect the higher-order ionospheric effects, there is most likely an underestimation in particular of the σ_{10}^{C}-coefficients based on solutions with $n_{\max} \leq 2$ (e.g., Lavallée et al. 2006). Taking $n_{\max} \geq 4$ (e.g., Wu et al. 2003) amplifies respective estimates.

Radiation pressure modeling effects

The interpretation of distinct constituents in the spectral domain of GPS parameter time series requires a thorough examination of an imperfect modeling of GPS observations. In particular, long-period variations in station position time series aliasing from residual subdaily tidal displacements (Penna et al. 2007; King et al. 2008) reach the level of millimeter. Ray et al. (2007) report anomalous harmonics in the spectra of GPS position estimates after removing an annual and semiannual term. Significant spectral power is found to be present for frequencies being multiples of 1.040 ± 0.008 cpy which are associated to the repeat time of the sun's position in space relative to the GPS orbital nodes as viewed from earth (351.4 days, corresponding to a frequency of 1.039 cpy). For this period, possible error sources are addressed relating to orbit mismodeling of solar radiation pressure acting on the GPS satellites (Hugentobler 2005). It should be emphasized that the older ROCK models (Fliegel et al. 1992; Fliegel and Gallini 1996) have been used in the past by individual IGS Analysis Centers, and thus, contributed to the final IGS products. Urschl et al. (2007) show a significant improvement of satellite laser ranging (SLR) range residuals for GPS satellites when applying the newer CODE model (Springer et al. 1999) developed at the Center for Orbit Determination in Europe (CODE). However, mismodeled short-period signals in GPS observations are shown to propagate to seasonal and near-annual periods caused by the alias mechanism that accompanies the repeating satellite constellation with respect to the tracking stations and the 24-h sampling used for GPS data processing (Penna and Stewart 2003; Agnew and Larson 2007).

We concentrate on the 351.4-day period because no related peaks are found in the respective spectra of SLR and very long baseline interferometry (VLBI) (Ray et al. 2007). We use reprocessed observations of the latest run for which the CODE radiation pressure model has been applied. In order to examine a possible systematic impact on the degree-1 coefficients, the same set of observations was processed with the ROCK models, instead. Since the spectral resolution based on 28-day samples of the reference frame solution is limited to multiples of the Nyquist period of 56 days, degree-1 estimates are derived with daily resolution based on the coordinate residual approach

(see "Coordinate residual approach"). Figure 6 (top) shows the resulting time series of $\Delta\mathbf{r}_{\mathrm{CF-CM}}$ computed with the CODE model (black line) and the ROCK models (red line). Whereas similar results are obtained for the x- and y-component, it is most important to note the difference in z. A spectral analysis is performed for the z-translation with respective amplitudes given in Fig. 6 (bottom). Almost all significant peaks seem to coincide with integer multiples of the basic frequency of 1.039 cpy. In comparison, larger peaks are obtained for the ROCK model-based series. This indicates an improvement when using the CODE model.

The length of the input time series and the daily sampling do not suffice to exactly sample neither the 1-cpy nor the 1.039-cpy frequency. A clear separation of both fractions is not possible based on the discrete Fourier spectra shown in Fig. 6. Therefore, a least-squares adjustment is performed accounting for the frequencies of interest. The related results are summarized in Table 2. Although periods belonging to 1 and 1.039 cpy are very close to each other, the length of our input time series of 14 years helps to discriminate both fractions. A notable finding is a significant reduction in amplitude in z for the 1.039-cpy part when applying the CODE model, more precisely 0.6 versus 2.9 mm. If annual contributions of 1 cpy are compared, another finding is that the series based on the ROCK models shows a phase bias of about 140 days and a slightly reduced amplitude, although the 1.039-cpy frequency has been adjusted for simultaneously. However, the phase in z, based on the CODE model, seems to be more realistic because it is in accordance with a positive degree-1 mass variation anomaly during the boreal winter (January/February) which has a clear geophysical meaning (Blewitt et al. 2001). In particular, our results show that more-frequently sampled degree-1 parameters do not prevent the radiation pressure-related observation residuals from causing an artificial annual σ_{10}^{C}-variation.

Comparison with GRACE satellite data

Time-variable surface mass redistribution is reflected in load deformations of the solid earth and in gravity field variations. Since these two signatures may be observed by data from GPS or GRACE, we directly compare our low-degree surface load coefficients to GRACE results. Unlike with GPS, degree-1 terms cannot be solved for by GRACE alone because the origin of the underlying reference system coincides with the center of mass of the earth system, that is the CM. Nevertheless, Swenson and Wahr (2008) estimate a time series of degree-1 surface load anomalies from a combination of GRACE satellite and ocean model data (ftp://podaac.jpl.nasa.gov/pub/tellus/monthly_

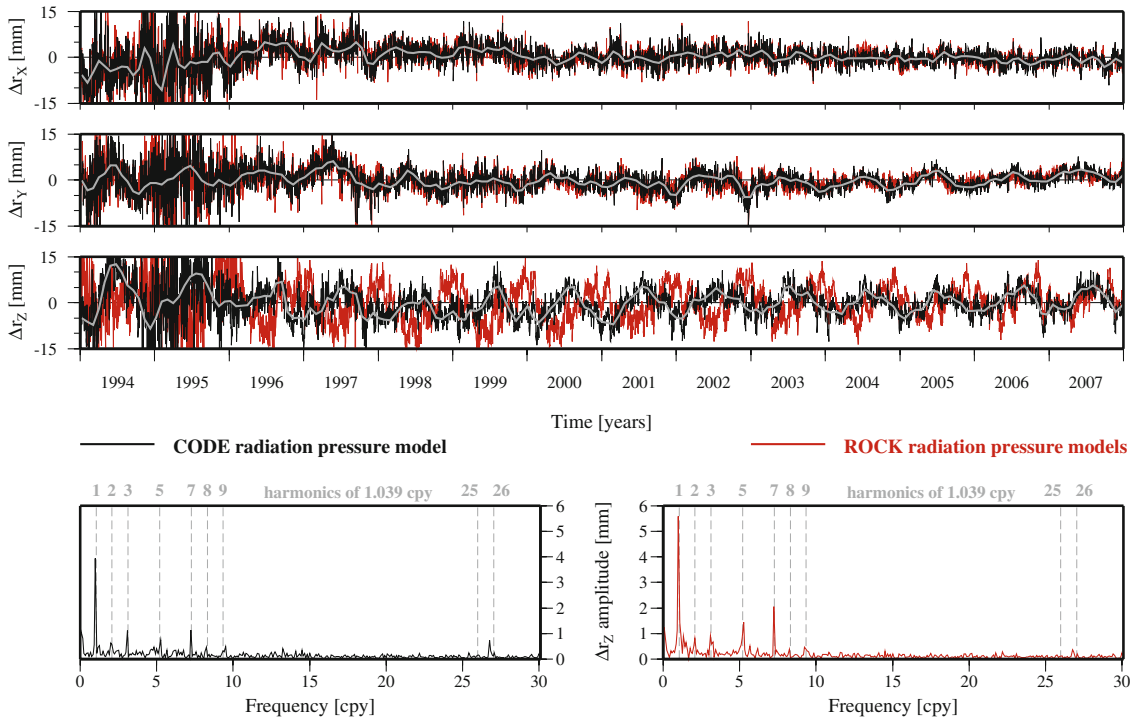

Fig. 6 Daily degree-1 estimates converted to the displacement of CF relative to CM, $\Delta\mathbf{r}_{\mathrm{CF-CM}}$. The results using the CODE and the ROCK radiation pressure models are shown in *black* and *red*, respectively. The reference solutions from "Rigorous combination approach" are superimposed in *gray*. The *bottom panels* show amplitudes of discrete Fourier spectra for the z-component only (limited range of frequencies shown here). Multiples of the basic frequency of 1.039 cpy are *highlighted*

Table 2 Amplitude and phase estimates based on daily CF displacements with respect to CM

Frequency (cpy)	$\Delta\mathbf{r}_{CF-CM}$					
	x		*y*		*z*	
	C	R	C	R	C	R
Amplitude (mm)						
1.000	0.3	0.6	**2.1**	**1.2**	**4.4**	**3.7**
1 × 1.039	0.3	0.1	0.4	0.3	**0.6**	**2.9**
5 × 1.039	0.1	0.1	0.2	0.2	0.3	1.3
7 × 1.039	0.1	0.2	0.1	0.1	1.0	1.9
Phase (days) with respect to first January 1994						
1.000	248	201	157	125	**207**	**348**
1 × 1.039	191	4	89	3	151	1
5 × 1.039	55	85	49	130	49	53
7 × 1.039	39	52	26	53	24	53

Common adjustment for an annual variation of 1 cpy and multiples of 1.039 cpy. See Fig. 6 for fractions with most power. The results refer to the application of the CODE (C) radiation pressure model and the ROCK (R) models. Notable differences are *highlighted*

mass_grids/chambers-destripe/dpc200711/degree_1_coeff/deg1_coef.txt). Figure 7 shows the respective degree-1 terms converted to $\Delta\mathbf{r}_{CF-CM}$ (red line) and our GPS-based results (black line). In comparison to their results for 2002.5–2008.0, we find similarities notably in *y* and *z*, although our GPS inversion does not incorporate any further constraints. Both amplitude and phase show a reasonable agreement. The correlation coefficients of corresponding time series are determined to be 0.52 for *y* and 0.57 for *z*. According to a trend in the GPS time series, the linear change of each component has been defined to be zero over the entire combination period 1994.0–2008.0 (see "Reference system realization"). Therefore, no additional trend has been subtracted from the GPS results shown in Fig. 7. However, due to long-term variations, a remaining trend seems to be obvious in *y* when looking just at the shorter time interval used for the comparison. Larger discrepancies are obtained for *x*, where the GPS inversion shows overall smaller amplitude, in particular for the later years. A correlation coefficient of −0.27 is obtained for this component. But, especially the estimation of this component suffers from the lack of contributing network sites in the Pacific region. Variations in the zonal term σ_{20}^{C} are obtained from our global GPS reanalysis as well and are shown in Fig. 7 (bottom, black line). We find a good agreement with the coefficients derived from GRACE data (http://isdc.gfz-potsdam.de; Schmidt et al. 2008), where the background fields were re-added to the GRACE solution (blue line). As to an obvious trend remaining for the GPS time series, the same is true for the σ_{20}^{C}-estimates as to the degree-1 estimates. A separate trend was not fitted for the time span of comparison; thus, the resulting correlation coefficient of about 0.43 is less significant.

Conclusion

We adjust reprocessed GPS observations to infer spherical harmonic coefficients of a surface mass redistribution. These estimates should be derived as a part of a rigorous parameter combination procedure where correlations between different parameters are accounted for correctly. In comparison, different results are obtained when applying an approach that solves for a linear model of site positions

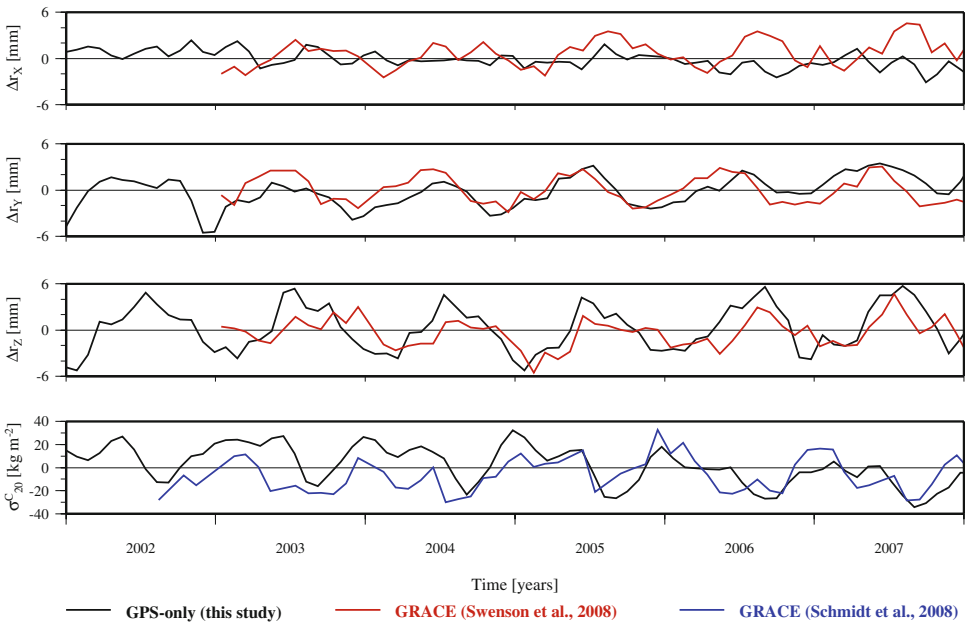

Fig. 7 Comparing GPS and GRACE solutions. The *top three panels* show the estimated degree-1 coefficients converted to the displacement $\Delta\mathbf{r}_{CF-CM}$. The pure spherical harmonic results from GPS are in *black* (this study), the GRACE data in combination with ocean bottom pressure data from model output are seen in *red* (Swenson and Wahr 2008). The *bottom panel* shows the zonal term σ_{20}^{C} from GPS in *black* and from GRACE GFZ RL04 data in *blue* (Schmidt et al. 2008)

and a time-dependent load-induced deformation separately. Derived differences in the displacement of CF and CM, i.e., $\Delta\mathbf{r}_{CF-CM}$, are on the order of 3 mm on average.

At present, the second and third-order ionospheric effects are still not taken into account for routinely generated products of the IGS. We show that neglecting higher-order ionospheric terms causes artificial long-term and semiannual variations for estimated degree-1 coefficients. If converted to $\Delta\mathbf{r}_{CF-CM}$, maximum discrepancies are on the order of 1.5 mm for the z-translation. That corresponds to approximately 25% of the magnitude of the annual amplitude of that component.

As described in detail, GPS-based degree-1 estimates are potentially biased by observation residuals originating from mismodeled dynamical sun–satellite interaction. Results presented in this study refer to the CODE radiation pressure model and reveal significantly reduced amplitudes for non-geophysical alias periods. Nevertheless, modeling deficiencies have to be identified first and taken into consideration before GPS inferred surface mass variations can be combined with results from GRACE or other space geodetic techniques such as SLR or VLBI.

The general approach of setting up surface load coefficients as additional parameters at the normal equation level can be adapted for variance–covariance solutions given in the solution independent exchange format (SINEX). In this case, station coordinate parameters must be explicitly provided, and free normal equations have to be derivable from the variance–covariance matrices. As a matter of fact, the latter condition requires that all solution constraints have to be removable. In particular, in the general solution, additional constraints must not be applied to parameters previously eliminated, such as satellite orbital and tropospheric parameters.

In conclusion, the estimation of additional quantities for redistributed surface loads concerns two major reference frame issues. First, a consistent description of load-induced surface deformation relative to the origin of the selected frame improves the accuracy and stability of that reference frame. Second, a consideration of these quantities in addition to site positions and earth rotation parameters for all contributing observation types in an intra-technique combination will provide a more consistent relation between all techniques and consequently will strengthen any combination product.

Acknowledgments We thank the International GNSS Service for providing the observation data via its data centers. Our sincere thanks go to the CODE Analysis Center team for their cooperation within the reprocessing project. This research was funded by the German Research Foundation (DFG). Figures were generated with the Generic Mapping Tools (http://gmt.soest.hawaii.edu/; Wessel and Smith 1991). The helpful comments of two anonymous reviewers are gratefully acknowledged.

References

Agnew D, Larson K (2007) Finding the repeat times of the GPS constellation. GPS Solut 11:71–76. doi:10.1007/s10291-006-0038-4

Altamimi Z, Collilieux X, Legrand J, Garayt B, Boucher C (2007) ITRF2005: a new release of the International Terrestrial Reference Frame based on time series of station positions and earth orientation parameters. J Geophys Res 112(B09401). doi:10.1029/2007JB004949

Blewitt G (2003) Self-consistency in reference frames, geocenter definition, and surface loading of the solid earth. J Geophys Res 108(B2):2103. doi:10.1029/2002JB002082

Blewitt G, Lavallée D, Clarke P, Nurutdinov K (2001) A new global mode of earth deformation: seasonal cycle detected. Science 294:2342–2345. doi:10.1126/science.1065328

Clarke P, Lavallée D, Blewitt G, van Dam T (2007) Basis functions for the consistent and accurate representation of surface mass loading. Geophys J Int 171(1):1–10. doi:10.1111/j.1365-246X.2007.03493.x

Dach R, Hugentobler U, Fridez P, Meindl M (eds) (2007) Bernese GPS software Version 5.0. Astronomical Institute, University of Bern, Switzerland

Davis JL, El'osegui P, Mitrovica JX, Tamisiea ME (2004) Climate-driven deformation of the solid earth from GRACE and GPS. Geophys Res Lett 31(L24605). doi:10.1029/2004GL021435

Dong D, Yunck T, Heflin M (2003) Origin of the International Terrestrial Reference Frame. J Geophys Res 108(B4):2200. doi:10.1029/2002JB002035

Dow JM, Neilan RE, Gendt G (2005) The International GPS Service (IGS): celebrating the 10th anniversary and looking to the next decade. Adv Space Res 36(3):320–326. doi:10.1016/j.asr.2005.05.125

Drewes H (2007) Science rationale of the global geodetic observing system (GGOS). In: Tregoning P, Rizos C (eds) IAG symposia 130 "Dynamic planet—monitoring and understanding a dynamic planet with geodetic and oceanographic tools", Springer, Berlin, pp 703–710, doi:10.1007/978-3-540-49350-1_101

Fliegel HF, Gallini TE (1996) Solar force modeling of block IIR global positioning system satellites. J Spacecr Rockets 33(6):863–866. doi:10.2514/3.26851

Fliegel HF, Gallini TE, Swift ER (1992) Global positioning system radiation force model for geodetic applications. J Geophys Res 97(B1):559–568. doi:10.1029/91JB02564

Fritsche M, Dietrich R, Knöfel C, Rülke A, Vey S, Rothacher M, Steigenberger P (2005) Impact of higher-order ionospheric terms on GPS estimates. Geophys Res Lett 32(L23311). doi:10.1029/2005GL024342

Heflin M, Watkins M (1999) Geocenter estimates from the global positioning system. In: IERS analysis campaign to investigate motions of the geocenter. IERS technical note no. 25, Obs. de Paris, Paris, pp 55–70

Hugentobler U (2005) Models in GNSS data analysis. Presentation at "Advances in GPS data processing and modelling for geodynamics" held at University College London, 9–10 November 2005 (available electronically at http://www.research.ge.ucl.ac.uk/COMET/)

King MA, Watson CS, Penna NT, Clarke PJ (2008) Subdaily signals in GPS observations and their effect at semiannual and annual periods. Geophys Res Lett 35(L03302). doi:10.1029/2007GL032252

Kusche J, Schrama EJO (2005) Surface mass redistribution inversion from global GPS deformation and gravity recovery and climate experiment (GRACE) gravity data. J Geophys Res 110(B09409). doi:10.1029/2004JB003556

Lavallée DA, van Dam T, Blewitt G, Clarke PJ (2006) Geocenter motions from GPS: a unified observation model. J Geophys Res 111(B05405). doi:10.1029/2005JB003784

McCarthy DD, Petit G (eds) (2004) IERS Conventions (2003). IERS technical note no. 32, Verlag des Bundesamts für Kartographie und Geodäsie, Frankfurt am Main, Germany

Penna NT, Stewart MP (2003) Aliased tidal signatures in continuous GPS height time series. Geophys Res Lett 30(23):2184. doi:10.1029/2003GL018828

Penna NT, King MA, Stewart MP (2007) GPS height time series: short-period origins of spurious long-period signals. J Geophys Res 112(B02402). doi:10.1029/2005JB004047

Ray J, Altamimi Z, Collilieux X, van Dam T (2007) Anomalous harmonics in the spectra of GPS position estimates. GPS Solut 12:55–64. doi:10.1007/s10291-007-0067-7

Rülke A, Dietrich R, Fritsche M, Rothacher M, Steigenberger P (2008) Realization of the terrestrial reference system by a reprocessed global GPS network. J Geophys Res 113(B08403). doi:10.1029/2007JB005231

Schmidt R, Flechtner F, Meyer U, Neumayer KH, Dahle C, König R, Kusche J (2008) Hydrological signals observed by the GRACE satellites. Surv Geophys 29:319–334. doi:10.1007/s10712-008-9033-3

Springer TA, Beutler G, Rothacher M (1999) A new solar radiation pressure model for GPS. Adv Space Res 23(4):673–676. doi:10.1016/S0273-1177(99)00158-1

Steigenberger P, Rothacher M, Dietrich R, Fritsche M, Rülke A, Vey S (2006) Reprocessing of a global GPS network. J Geophys Res B05402(111). doi:10.1029/2005JB003747

Swenson S, Wahr J (2008) Estimating geocenter variations from a combination of GRACE and ocean model ouput. J Geophys Res 113(B08410). doi:10.1029/2007JB005338

Urschl C, Beutler G, Gurtner W, Hugentobler U, Stefan S (2007) Contribution of SLR tracking data to GNSS orbit determination. Adv Space Res 39(10):1515–1523. doi:10.1016/j.asr.2007.01.038

van Dam T, Wahr J, Lavallée D (2007) A comparison of annual vertical crustal displacements from GPS and gravity recovery and climate experiment (GRACE) over Europe. J Geophys Res 112(B03404). doi:10.1029/2006JB004335

Wessel P, Smith WHF (1991) Free software helps map and display data. Eos Trans AGU 72:441. doi:10.1029/90EO00319

Wu X, Argus DF, Heflin MB, Ivins ER, Webb FH (2002) Site distribution and aliasing effects in the inversion for load coefficients and geocenter motion from GPS data. Geophys Res Lett 29(24):2210. doi:10.1029/2002GL016324

Wu X, Heflin MB, Ivins ER, Argus DF, Webb FH (2003) Large-scale global surface mass variations inferred from GPS measurements of load-induced deformation. Geophys Res Lett 30(14):1742. doi:10.1029/2003GL017546

Wu X, Heflin MB, Ivins ER, Fukumori I (2006) Seasonal and interannual global surface mass variations from multisatellite geodetic data. J Geophys Res 111(B09401). doi:10.1029/2005JB004100